Electrochimica Acta 55 (2010) 6218–6227

Contents lists available at ScienceDirect

Electrochimica Acta

journal homepage: www.elsevier.com/locate/electacta

Determination of effective capacitance and film thickness from constant-phase-element parameters

Bryan Hirschorn[a], Mark E. Orazem[a,*], Bernard Tribollet[b], Vincent Vivier[b], Isabelle Frateur[c], Marco Musiani[d]

[a] Department of Chemical Engineering, University of Florida, Gainesville, FL 32611, USA
[b] LISE, UPR 15 du CNRS, Université P. et M. Curie, CP 133, 4 Place Jussieu, 75252 Paris cedex 05, France
[c] Laboratoire de Physico-Chimie des Surfaces, UMR CNRS-ENSCP 7045, École Nationale Supérieure de Chimie de Paris, 11 rue Pierre et Marie Curie, 75005 Paris, France
[d] Istituto per l'Energetica e le Interfasi, IENI - CNR, Corso Stati Uniti 4, 35127 Padova, Italy

ARTICLE INFO

Article history:
Received 24 July 2009
Received in revised form 26 October 2009
Accepted 27 October 2009
Available online 13 November 2009

Keywords:
Impedance spectroscopy
Niobium oxide
Human stratum corneum
Constant-phase element
Young model
Time-constant distribution

ABSTRACT

Two different mathematical formulas for estimating effective capacitance from Constant-Phase-Element (CPE) parameters, taken from the literature, are associated unambiguously with either surface or normal time-constant distributions. Application to different systems are used to illustrate the importance of using the correct formula that corresponds to a given type of distribution. Experiments and simulations are used to show that the effective capacitance obtained for a normal distribution yields correct values for the film thickness under conditions where the local resistivity does not vary significantly. When the local resistivity varies considerably over the thickness of a film, the experimental frequency range may preclude observation of the capacitance contribution of a portion of the film, resulting in under prediction of the film thickness.

1. Introduction

The impedance response for electrochemical systems often reflects a distribution of reactivity that is commonly represented in equivalent electrical circuits as a constant-phase element (CPE) [1–3]. The impedance associated with a simple Faradaic reaction without diffusion can be expressed in terms of a CPE as

$$Z(\omega) = R_e + \frac{R_t}{1 + (j\omega)^{\alpha} Q R_t} \tag{1}$$

where R_e is the Ohmic resistance and R_t is the charge-transfer resistance. The CPE parameters α and Q are independent of frequency. When $\alpha = 1$, Q has units of a capacitance, i.e., $\mu F/cm^2$, and represents the capacity of the interface. When $\alpha < 1$, the system shows behavior that has been attributed to surface heterogeneity [4,5] or to continuously distributed time constants for charge-transfer reactions [6–10]. Independent of the cause of CPE behavior, the phase angle associated with a CPE is independent of frequency. For a blocking electrode, Eq. (1) can be expressed as

$$Z(\omega) = R_e + \frac{1}{(j\omega)^{\alpha} Q} \tag{2}$$

where Q represents the differential capacity of the interface in the case where $\alpha = 1$.

It is clear that the CPE parameter Q cannot represent the capacitance when $\alpha < 1$. A number of researchers have explored the relationship between CPE parameters and the interfacial capacitance. By treating a surface distribution of time constants, Brug et al. [1] developed relationships between interfacial capacitance and CPE parameters for both blocking and Faradaic systems. Hsu and Mansfeld [11] proposed a different relationship in terms of Q, α and ω_{max}, which is the characteristic frequency at which the imaginary part of the impedance reaches its maximum magnitude.

The formulas yield different results for the effective capacitance. Using numerical simulations for the influence of geometry-induced current distributions, Huang et al. [12] have shown that current and potential distributions induce a high-frequency pseudo-CPE behavior in the global impedance response of a disk electrode with a Faradaic reaction [13]. Their work demonstrated that the Brug formula for effective capacitance yielded a more accurate estimate than did the Hsu and Mansfeld equation.

* Corresponding author at: Department of Chemical Engineering, University of Florida, PO Box 116005, Gainesville, FL 32611, USA.
E-mail address: meo@che.ufl.edu (M.E. Orazem).

0013-4686/$ – see front matter © 2009 Elsevier Ltd. All rights reserved.
doi:10.1016/j.electacta.2009.10.065

Both the Brug formulas and the Hsu and Mansfeld formula have been widely used to extract effective capacitance values from CPE parameters. The Brug formulas have been used to extract capacitance values from CPE parameters for studies on double layers [14–18], hydrogen sorption in metals [19,20], hydrogen evolution [21–26], oxygen evolution [27], porous electrodes [28], self-assembled monolayers [29,30], polymer films [31], and passive films [32,33]. Similarly, the Hsu and Mansfeld formula has been used to extract capacitance values from CPE parameters for studies on passive films [32–34], protective coatings [35–38], and corrosion inhibitors [39]. For a given set of CPE parameters, the Brug formulas and the Hsu and Mansfeld formula yield different values; yet, in some cases, both sets of equations have been applied to similar systems. The objective of this work is to explore the conditions of validity for models which relate capacitance to CPE parameters.

2. Applicability of capacitance–CPE relations

Two types of time-constant distributions are envisioned. A variation of properties along the surface of an electrode can give rise to a time-constant dispersion, which, for an appropriate distribution function, may be expressed as a CPE. A variation of properties normal to the surface of an electrode can also give rise to a time-constant dispersion, which, for an appropriate distribution function, may be expressed as a CPE.

2.1. Surface distributions

In the case of a surface time-constant distribution, the global admittance response of the electrode must include additive contributions from each part of the electrode surface. The situation is demonstrated in Fig. 1(a), where a surface distribution of time constants in the presence of an Ohmic resistance results in a distributed time-constant behavior expressed as a summation of admittances. For an appropriate time-constant distribution, the impedance response may be expressed in terms of a CPE. Interestingly, in the absence of an Ohmic resistance, shown in Fig. 1(b), the surface distribution of time constants results in an effective *RC* behavior in which

$$\frac{1}{R_{\text{eff}}} = \sum \frac{1}{R_i} \tag{3}$$

and

$$C_{\text{eff}} = \sum C_i \tag{4}$$

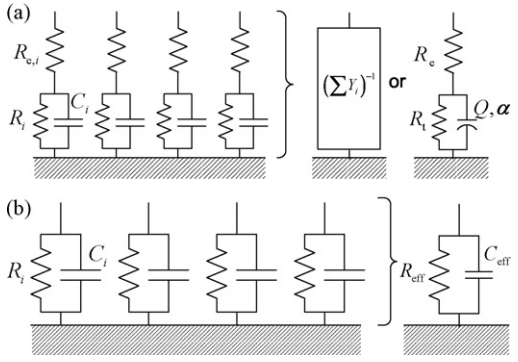

Fig. 1. Schematic representation of a surface distribution of time constants: (a) distribution of time constants in the presence of an Ohmic resistance resulting in a distributed time-constant behavior that, for an appropriate time-constant distribution, may be expressed as a CPE; and (b) distribution of time constants in the absence of an Ohmic resistance resulting in an effective RC behavior. The admittance Y_i shown in (a) includes the local interfacial and Ohmic contributions.

Thus, the appearance of a CPE behavior associated with a surface distribution of time constants requires the contribution of an Ohmic resistance [40,41]. While an Ohmic resistance in physical systems cannot be avoided, the example illustrated in Fig. 1(b) illustrates the crucial role played by the Ohmic resistance in CPE behavior associated with surface distributions.

Following the development of Brug et al. [1], the relationship between CPE parameters and effective capacitance requires an assessment of the characteristic time constant corresponding to the admittance of the electrode. Thus,

$$Y = \sum_i Y_i = \sum_i \left(R_{e,i} + \frac{R_i}{1 + j\omega R_i C_i} \right)^{-1} \tag{5}$$

where Y_i is the local admittance represented in Fig. 1(a), $R_{e,i}$ is the local Ohmic resistance and R_i and C_i represent the local surface properties. On the other hand, the total admittance of the electrode can also be expressed in terms of the CPE represented by Eq. (1) as

$$Y = \frac{1}{R_e} \left[1 - \frac{R_t}{R_e + R_t} \left(1 + \frac{R_e R_t}{R_e + R_t} Q(j\omega)^{\alpha} \right)^{-1} \right] \tag{6}$$

where R_e is the global Ohmic resistance and R_t, Q, and α represent global properties. Eq. (6) can be expressed in terms of a characteristic time constant τ_0 as

$$Y = \frac{1}{R_e} \left[1 - \frac{R_t}{R_e + R_t} \left(1 + (j\omega\tau_0)^{\alpha} \right)^{-1} \right] \tag{7}$$

where

$$\tau_0 = \frac{R_e R_t}{R_e + R_t} C_{\text{eff}} \tag{8}$$

Comparison of Eqs. (6) and (7) yields

$$\tau_0^{\alpha} = Q \frac{R_e R_t}{R_e + R_t} = Q \left(\frac{1}{R_e} + \frac{1}{R_t} \right)^{-1} \tag{9}$$

The effective capacitance associated with the CPE can therefore be expressed as

$$C_{\text{eff}} = Q^{1/\alpha} (R_e^{-1} + R_t^{-1})^{(\alpha-1)/\alpha} \tag{10}$$

or

$$C_{\text{eff}} = Q^{1/\alpha} \left(\frac{R_e R_t}{R_e + R_t} \right)^{(1-\alpha)/\alpha} \tag{11}$$

Eqs. (10) and (11) are equivalent to Eq. (20) derived by Brug et al. [1] for a surface distribution with a different definition of CPE parameters. In the limit that R_t becomes infinitely large, Eq. (11) becomes

$$C_{\text{eff}} = Q^{1/\alpha} R_e^{(1-\alpha)/\alpha} \tag{12}$$

which is equivalent to Eq. (5) presented by Brug et al. [1] for a blocking electrode.

2.2. Normal distributions

In the case of a normal time-constant distribution through a surface layer, the global impedance response of the electrode must include additive contributions from each part of the layer. The situation is demonstrated in Fig. 2, where a normal distribution of time constants results in a distributed time-constant behavior expressed as a summation of impedances. For an appropriate time-constant distribution, the impedance response may be expressed in terms of a CPE. In this case, the appearance of a CPE behavior does not require the contribution of an Ohmic resistance. The appearance of a CPE from a series of Voigt *RC* elements does, however, require contributions from both resistive and capacitive elements.

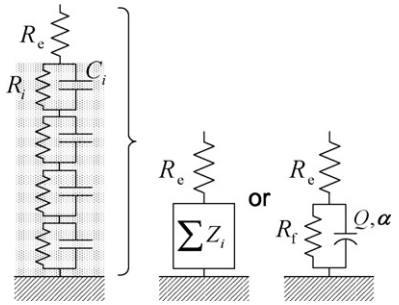

Fig. 2. Schematic representation of a normal distribution of time constants resulting in a distributed time-constant behavior that, for an appropriate time-constant distribution, may be expressed as a CPE.

The relationship between CPE parameters and effective capacitance requires an assessment of the characteristic time constant corresponding to the impedance of the layer. Thus,

$$Z = R_e + \sum_i Z_i = R_e + \sum_i \frac{R_i}{1 + j\omega R_i C_i} \tag{13}$$

where R_e is the Ohmic resistance and R_i and C_i represent the local properties of the layer. Since the Ohmic resistance does not contribute to the time-constant dispersions of a film, the development can be performed in terms of an Ohmic resistance-corrected impedance $Z - R_e$.

The Ohmic resistance-corrected impedance of a film can be expressed in terms of a CPE as

$$Z - R_e = \frac{R_f}{1 + (j\omega)^\alpha Q R_f} \tag{14}$$

where

$$R_f = \sum_i R_i \tag{15}$$

represents the film resistance. Alternatively,

$$Z - R_e = \frac{R_f}{1 + (j\omega\tau_0)^\alpha} \tag{16}$$

Comparison of Eqs. (14) and (16) yields

$$\tau_0^\alpha = (R_f C_{eff})^\alpha = Q R_f \tag{17}$$

The effective capacitance associated with the CPE can therefore be expressed as

$$C_{eff} = Q^{1/\alpha} R_f^{(1-\alpha)/\alpha} \tag{18}$$

Eq. (18) is equivalent to Eq. (3) presented without derivation by Hsu and Mansfeld [11] in terms of ω_{max}. Eqs. (11), (12), and (18) have all the same form, but the resistance used in the calculations of C_{eff} is different in the three cases, being, respectively, the parallel combination of R_t and R_e for Eq. (11), R_e for Eq. (12) and R_f for Eq. (18).

3. Application

Eqs. (11), (12), and (18) were applied to different surface and normal distributions for determination of effective capacitance.

3.1. Surface distributions

Huang et al. [12] have shown that current and potential distributions induce a high-frequency pseudo-CPE behavior in the global impedance response of an ideally polarized blocking electrode with a local ideally capacitive behavior. In a related work, Huang et al. [42] explored the role of current and potential distributions on the global and local impedance responses of a blocking electrode exhibiting a local CPE behavior. They were able to relate the global impedance response to local impedance, and distinctive features of the calculated global and local impedance response were verified experimentally. A similar development was presented for a disk electrode with a Faradaic reaction [13].

This work was used to explore the applicability of Eqs. (11), (12), and (18) for determination of effective capacitance. The approach allowed comparison between the estimated capacitance and the value assumed for the simulations. The graphical methods presented by Orazem et al. [43] were used to obtain CPE parameters α and Q_{eff}. The parameter α was obtained from

$$\alpha = \left| \frac{d \log |Z_j|}{d \log f} \right| \tag{19}$$

and Q_{eff} was obtained from

$$Q_{eff} = \sin\left(\frac{\alpha\pi}{2}\right) \frac{-1}{Z_j \omega^\alpha} \tag{20}$$

The parameters α and Q_{eff} obtained by graphical evaluation of Eqs. (19) and (20) are the same as would be obtained by regression analysis. As discussed by Huang et al. [13], the frequencies used for the analysis were limited to those that were one decade larger than the characteristic frequency because, in this frequency range, the value of α was well-defined. The analysis took into account the observation that the value of α was dependent on the frequency at which the slope was evaluated.

The value of effective CPE coefficient, Q_{eff}, scaled by the interfacial capacitance C_0 used for the simulations, is presented in Fig. 3 as a function of dimensionless frequency $K = \omega C_0 r_0/\kappa$, where r_0 is the disk radius, and κ is the conductivity of the electrolyte. The results given in Fig. 3 are presented as a function of the parameter J, incorporated as part of the boundary condition for Faradaic reactions at the electrode surface. Under the assumption of linear kinetics, valid for steady-state current densities $\bar{i}$ much smaller than the exchange current density i_0, the parameter J was defined to be

$$J = \frac{(\alpha_a + \alpha_c) F i_0 r_0}{RT\kappa} \tag{21}$$

where α_a and α_c are, respectively, anodic and cathodic apparent transfer coefficients. For Tafel kinetics, valid for $\bar{i} \gg i_0$, the parameter J was defined to be a function of radial position on the electrode surface as

$$J(r) = \frac{\alpha_c F \left|\bar{i}(r)\right| r_0}{RT\kappa} \tag{22}$$

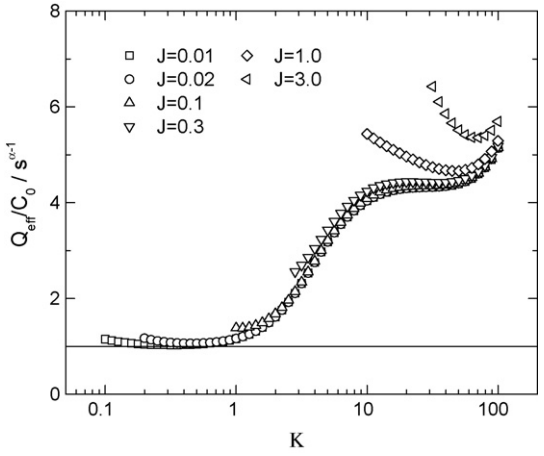

Fig. 3. Effective CPE coefficient scaled by the interfacial capacitance as a function of dimensionless frequency K with J as a parameter. Taken from Huang et al. [13].

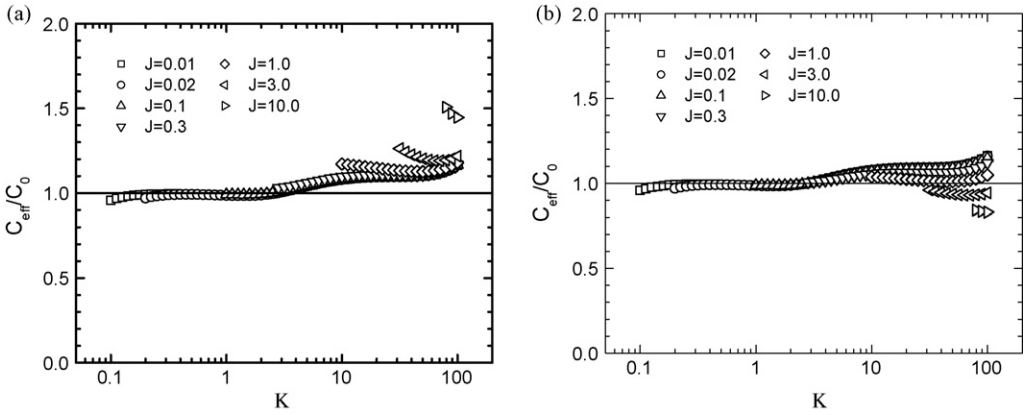

Fig. 4. Normalized effective capacitance calculated from relationships presented by Brug et al. [1] for a disk electrode as a function of dimensionless frequency K with J as a parameter: (a) with correction for Ohmic resistance R_e (Eq. (12)); and (b) with correction for both Ohmic resistance R_e and charge-transfer resistance R_t (Eq. (11)). Taken from Huang et al. [13].

where $\bar{i}(r)$ was obtained from the steady-state solution as

$$\bar{\imath}(r) = -i_0 \exp\left(-\frac{\alpha_c F}{RT}(\bar{V} - \bar{\Phi}_0(r))\right) \quad (23)$$

where $\bar{V} - \bar{\Phi}_0(r)$ represents the local interfacial potential driving force for the reaction.

The parameter J can be expressed in terms of the Ohmic resistance R_e and charge-transfer resistance R_t as

$$J = \frac{4}{\pi}\frac{R_e}{R_t} \quad (24)$$

Large values of J are seen when the Ohmic resistance is much larger than the charge-transfer resistance, and small values of J are seen when the charge-transfer resistance dominates. At high frequencies, where frequency dispersion plays a significant role, the effective CPE coefficient Q_{eff} provides an inaccurate estimate for the interfacial capacitance used as an input for the simulations, even for small values of J where, as shown by Huang et al. [13], α is close to unity. As shown in Fig. 3, assumption that Q_{eff} represents the interfacial capacitance results in errors on the order of 500% at $K = 100$.

Eqs. (12) and (11) are compared to the expected value of interfacial capacitance in Figs. 4(a) and (b), respectively. Following the observation by Huang et al. [13] that the geometry-induced potential and current distributions yield a pseudo-CPE behavior in which the coefficient α is a weak function of frequency, Figs. 4(a) and (b) was developed using frequency-dependent values of α and Q_{eff}. Thus, the value of Q_{eff} reported is that corresponding to the value of α at a given frequency K. The error in Eq. (12) is a function of both frequency K and J. While Eq. (12) applies strictly for a blocking electrode, it gives the correct answer for Faradaic systems if one chooses to calculate α at frequencies $K < 5$, but fails for $K > 5$. The dependence on J is reduced significantly when both the Ohmic resistance R_e and charge-transfer resistance R_t are taken into account, and the errors in estimating interfacial capacitance are less than 20%. The correction for R_t in Eq. (11) is important for frequencies $K > 5$. Of the relationships tested, Eq. (11) provides the best means for estimating interfacial capacitance when frequency dispersion is significant.

Eq. (18) was tested against the input value of interfacial capacitance in Fig. 5 where C_0 is the known interfacial capacitance. While Eq. (18) represents an improvement as compared to direct use of the CPE coefficient Q_{eff}, the errors in estimating the interfacial capacitance depend on both J and K and range between −70% and +100%. Eq. (18), developed for a normal time-constant distribution, is not appropriate for interpretation of results affected by a surface time-constant distribution.

3.2. Normal distributions

Eq. (18), developed for normal time-constant distributions, was applied for determination of effective capacitance in two systems in which a normal variation of resistivity may be expected.

3.2.1. Niobium

The anodic dissolution of a 0.25 cm^2 Nb (99.9%, Goodfellow) rotating disk electrode was studied in a pH 2 solution containing 0.1 M NH_4F and sodium sulfate as supporting electrolyte [44]. The experimental impedance data corresponding to an anodization potential of 6 V(SCE) are shown in Fig. 6(a). According to the "surface charge approach" developed by Bojinov [45,46], the dielectric properties of the oxide film dominate the high-frequency response. The medium-frequency inductive loop and low-frequency capacitive line are also described by Cattarin et al. [44] and Frateur [47]. Fig. 6(b) shows that a plot of the logarithm of the imaginary part of the impedance as a function of the logarithm of the frequency yields a straight line with a slope of −0.90 for frequencies higher than 300 Hz, which indicates a CPE behavior with a CPE exponent of 0.90 [43], rather than the response of a true R_fC_f parallel combination, where R_f is the oxide film resistance and C_f is the oxide film capacitance. Furthermore, in Fig. 6(b), the surface distribution caused by non-uniform current and potential distributions cannot be observed in the high-frequency range since $K = 1$ would corre-

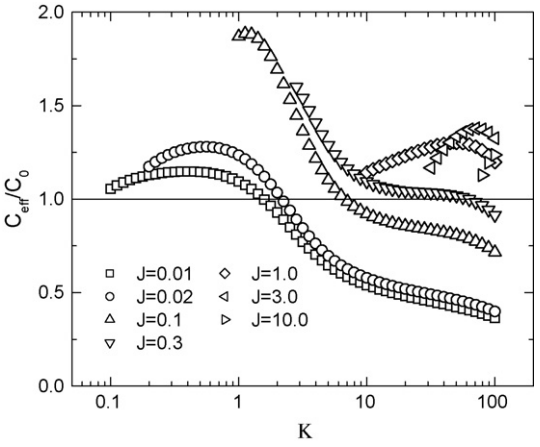

Fig. 5. Effective capacitance calculated from Eq. (18) and normalized by the input interfacial capacitance for a disk electrode as a function of dimensionless frequency K with J as a parameter. Taken from Huang et al. [13].

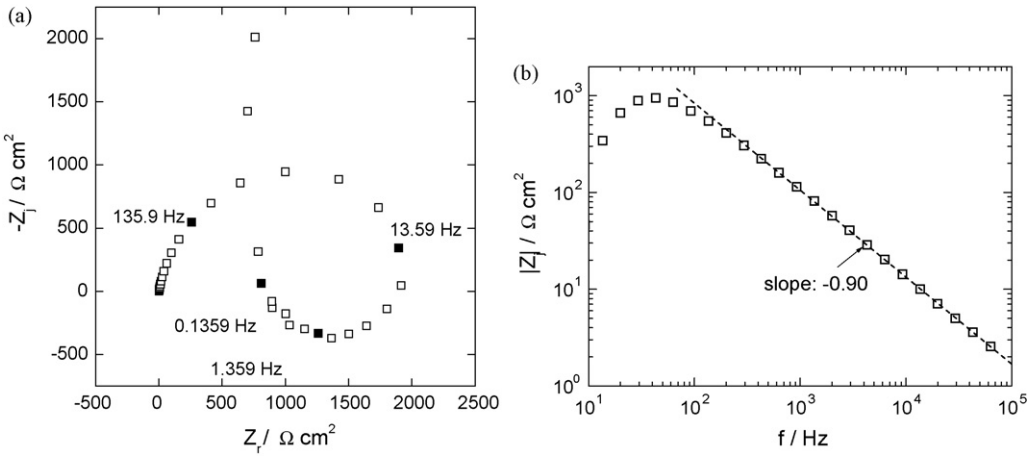

Fig. 6. Experimental impedance data obtained with a Nb rotating disk electrode (900 rpm) in 0.1 M NH_4F solution (pH 2), at 6 V(SCE): (a) complex plane plot; and (b) the imaginary part of the impedance as a function of frequency. Data taken from Cattarin et al. [44].

spond to 65 kHz and the maximum frequency that was used in the experiments was 63.1 kHz [42].

The CPE parameters α and Q for the high-frequency loop were obtained using the graphical methods presented by Orazem et al. [43] (Eqs. (19) and (20), respectively). The resulting values for different anodization potentials are presented in Table 1. The values of the oxide film resistance corresponding to the diameter of the high-frequency loop are also reported in Table 1. From the CPE parameters and the film resistance, the effective capacitance of the oxide film was determined by application of Eq. (18) (see Table 1).

For normal time-constant distributions for which the dielectric constant may be assumed to be independent of position, the capacitance should be related to film thickness d_{eff} according to

$$C_{eff} = \frac{\varepsilon\varepsilon_0}{d_{eff}} \quad (25)$$

where ε is the dielectric constant and $\varepsilon_0 = 8.8542 \times 10^{-14}$ F/cm is the permittivity of vacuum. In the case of anodic dissolution of Nb in acid fluoride medium, the oxide is assumed to be Nb_2O_5 and $\varepsilon = 42$ [48,49]. The values of d_{eff} are presented in Table 1 for different anodization potentials.

The calculated values of d_{eff} can be compared to those given in the literature. In Lohrengel's review of metal oxides [50], different values for the thickness of Nb_2O_5 films formed on Nb electrodes at $E = 0$ V(SHE) are given that vary between 3 and 6.7 nm. Moreover, the formation ratio (i.e., the thickness increase caused by a unit increase of the polarization potential) is reported to be 2.6 or 2.8 nm/V. Therefore, according to Lohrengel [50], the thickness δ can be estimated approximately to be $\delta = 5.0 + 2.70E$ where δ has units of nm and E is expressed in V(SHE). The method(s) used to determine the oxide film thicknesses and the electrolyte composition are not mentioned in Ref. [50]. Arsova et al. [51] measured the thickness of Nb_2O_5 films formed in 1 M H_2SO_4 by ellipsometry. The formation ratio determined by these authors is 2.26 nm/V. Extrapolation of their δ to $E = 0$ V yields $\delta = 5$ nm. Therefore, the thickness found by Arsova et al. [51] can be estimated to be $\delta = 5.0 + 2.26E$ where δ has units of nm and E is expressed in V(SHE). Habazaki et al. [52] measured the thickness of the oxide by TEM of an ultramicrotomed section and by impedance. From their data, the thickness can be estimated to be $\delta = 2.4 + 2.08E$ where δ has units of nm and E is referenced to Pt in 0.1 M H_3PO_4. The values of Nb_2O_5 film thickness calculated by using Eqs. (18) and (25) for different anodization potentials are compared with those calculated from the data of Lohrengel [50], Arsova et al. [51] and Habazaki et al. [52] in Table 2. The values of d_{eff} calculated by application of Eqs. (18) and (25) to impedance data are in very good agreement with the literature values, in particular with those obtained from non-electrochemical measurements. Our results agree also with those of Heidelberg et al. [53] who reported on the oxidation of 10 nm thick Nb layers in micro- and nano-cells.

To show the consequence of the misuse of the resistance term in the calculation of the effective capacitance, the values of C_{eff} were calculated using Eq. (11) in which R_t was replaced by R_f. Eq. (12) yielded the same values for C_{eff} as Eq. (11) since $R_f \gg R_e$. As before, Eq. (25) was used to estimate d_{eff}. Use of Eq. (12) yielded: for 2 V(SCE), $C_{eff} = 3.2$ μF/cm^2 and $d_{eff} = 12$ nm, for 6 V(SCE), $C_{eff} = 0.9$ μF/cm^2 and $d_{eff} = 41$ nm, and for 10 V(SCE), $C_{eff} = 0.5$ μF/cm^2 and $d_{eff} = 74$ nm. Comparison to the values presented in Table 1 shows that the effective film thickness obtained using the effective capacitance obtained from Eq. (12) can be significantly larger than the actual film thickness, especially at high potential.

3.2.2. Human skin

Impedance data were collected for heat-separated excised human stratum corneum obtained from the abdomen or the back [54]. The separation procedure involved physical and mechanical manipulations to separate the stratum corneum from the underlying dermis. Deionized water was the only solvent added during the process. The skin samples were mounted between glass diffusion cells prior to the impedance study. The skin and the solution were

Table 1
CPE parameters, resistance, effective capacitance, and thickness of oxide films formed on a Nb disk electrode in 0.1 M NH_4F solution (pH 2) as a function of the anodization potential.

Potential/ V(SCE)	α	Q /Ω^{-1} cm^{-2} s$^{\alpha}$	R_f/kΩ cm^2	C_{eff}/μF cm^{-2}	d_{eff}/nm
2	0.95	5.9×10^{-6}	1.30	4.6	8
6	0.90	3.5×10^{-6}	2.01	2.0	18
10	0.88	2.5×10^{-6}	3.65	1.3	29

Table 2
Thickness of oxide films developed on a Nb electrode, as a function of the anodization potential. Comparison of values deduced from impedance data with those from the literature.

Potential/V(SCE)	Present work	Values from literature		
	d_{eff}/nm	δ/nm [50]	δ/nm [51]	δ/nm [52]
2	8	11	10	7
6	18	22	19	15
10	29	33	28	24

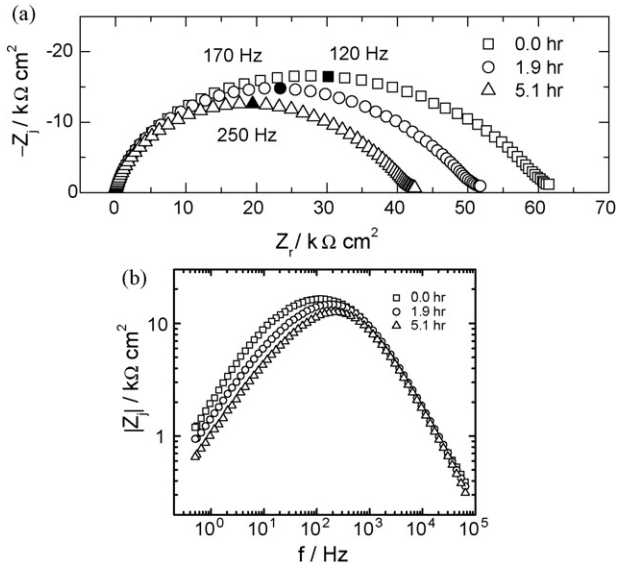

Fig. 7. Experimental impedance data obtained for heat-separated excised human stratum corneum in 50 mM buffered $CaCl_2$ electrolyte with immersion time as a parameter: (a) complex plane plot; and (b) the imaginary part of the impedance as a function of frequency. Data taken from Membrino [54].

maintained at constant temperature of 32 ° C with a water-jacketed diffusion cell. Magnetic stir bars were used for each chamber of the diffusion cell to keep the solutions well mixed. The electrochemical impedance measurements were conducted with a Solartron 1286 potentiostat and a Solartron 1250 frequency-response analyzer. A four-electrode configuration was used for all of the studies. The Ag/AgCl counter and working electrodes were produced by In Vivo Metric. The Ag/AgCl reference electrodes were fabricated by Micro Electrodes, Inc.

The slightly moistened epidermis was stored in between two sheets of polymer film in a refrigerator. At the start of a typical experiment the skin was removed from the refrigerator and immersed in a 32 ° C 50 mM $CaCl_2$/20 mM HEPES solution (pH of 6.95) which provided approximately the same pH and ionic strength as the electrolytic fluid within the body [55]. Replicate electrochemical impedance spectra were collected periodically using Variable-Amplitude Galvanostatic (VAG) modulation [56,57]. The sinusoidal current perturbation was superimposed about a 0 μA DC current bias, and the amplitude of the potential response across the skin was maintained at ±10 mV. The individual scans took approximately 5 min and were shown to satisfy the Kramers–Kronig relations, indicating that the system was stationary on the time scale of the experiments. Upon completion of an impedance scan the skin was allowed to relax for 3 min before the replicated spectrum was collected.

Impedance results are presented in Fig. 7(a) with immersion time as a parameter. The straight lines evident at high frequencies in Fig. 7(b) show a high-frequency constant-phase behavior. The CPE parameters α and Q were obtained using the graphical methods presented by Orazem et al. [43]. The resulting values for different immersion times are presented in Table 3. The value of

Table 3
CPE parameters, resistance, effective capacitance, and thickness for heat-stripped human stratum corneum in 50 mM buffered $CaCl_2$ electrolyte as a function of immersion time. Data taken from Membrino [54].

Time/h	α	Q /Ω^{-1} cm^{-2} s$^{\alpha}$	R_f/kΩ cm^2	C_{eff}/μF cm^{-2}	d_{eff}/μm
0.0	0.824	6.13×10^{-8}	60	1.86×10^{-2}	2.3
1.9	0.834	5.36×10^{-8}	51	1.66×10^{-2}	2.6
5.1	0.838	5.40×10^{-8}	42	1.66×10^{-2}	2.6

the thickness of the skin depends on its dielectric constant ε. The estimated thicknesses d_{eff} reported in Table 3 were obtained from Eqs. (18) and (25) under the assumption that $\varepsilon = 49$. The value of dielectric constant used in the present work was obtained by the comparison, shown in a subsequent section, of the Young model to the impedance data. The resulting values of d_{eff} of around 2 μm are substantially smaller than the thickness of the stratum corneum, which is accepted to have a value between 10 and 40 μm [58].

Eq. (12) was also used to calculate the effective capacitance. As for the case of Nb_2O_5, Eq. (11) yielded similar values for C_{eff} as Eq. (12) since $R_f \gg R_e$. Eq. (25) was used to estimate d_{eff}. Use of Eq. (12) yielded: for 0.0 h, $C_{eff} = 4.5 \times 10^{-3}$ μF/cm^2 and $d_{eff} =$ 9.6 μm, for 1.9 h, $C_{eff} = 3.7 \times 10^{-3}$ μF/cm^2 and $d_{eff} = 12$ μm, and for 5.1 h, $C_{eff} = 3.1 \times 10^{-3}$ μF/cm^2 and $d_{eff} = 14$ μm. Interestingly, the effective film thickness calculated using the effective capacitance obtained from Eq. (12) was closer to the expected value than was the thickness estimated using Eq. (18). The apparent better agreement is found in spite of the fact that the Ohmic resistance R_e has no relationship to the dielectric property of the skin. This work illustrates a need for a better understanding of the influence of strong variations of resistivity on the impedance response.

3.2.3. Films with an exponential decay of resistivity

The values of d_{eff} calculated using Eqs. (18) and (25) were in very good agreement with the literature values for Nb_2O_5 films, but the values obtained for human stratum corneum were substantially smaller than the expected values. Both the niobium oxide [47,59,60] and the skin systems [61,62] have been described as having a resistivity that decays exponentially with position. The case of a film with a uniform dielectric constant and an exponential decay of local resistivity is mathematically equivalent to the Young model, in which an exponential increase in conductivity is assumed [59,60]. The local resistance $R(x)$ can be expressed as

$$R(x) = \rho_0 e^{-x/\lambda}\, dx \tag{26}$$

where ρ_0 is the maximum value of resistivity found at $x = 0$, which corresponds to the oxide–electrolyte interface, and λ represents a characteristic length. The effective resistance of the film can be obtained by integration over the film thickness δ, i.e.,

$$R_{eff} = \int_0^{\delta} \rho_0 e^{-x/\lambda}\, dx \tag{27}$$

to yield

$$R_{eff} = \rho_0 \lambda \left(1 - e^{-\delta/\lambda}\right) \tag{28}$$

The local capacitance can be expressed as

$$C(x) = \frac{\varepsilon \varepsilon_0}{dx} \tag{29}$$

where the dielectric constant ε was assumed to have a uniform value. The effective capacitance, obtained by integration over the film thickness, following

$$\frac{1}{C_{eff}} = \int_0^{\delta} \frac{1}{\varepsilon \varepsilon_0} dx \tag{30}$$

is found to be

$$C_{eff} = \frac{\varepsilon \varepsilon_0}{\delta} \tag{31}$$

Eq. (31) is identical to Eq. (25), as the integration is valid for all dielectrics.

The impedance of the film is obtained from integration across the film thickness following

$$Z = \int_0^{\delta} \frac{\rho_0 e^{-x/\lambda}}{1 + j\omega \rho_0 e^{-x/\lambda} \varepsilon \varepsilon_0} dx \tag{32}$$

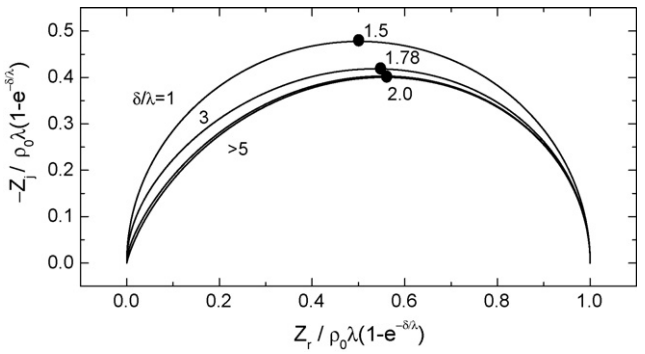

Fig. 8. Nyquist plots for simulation of the impedance associated with an exponential decay of resistivity with δ/λ as a parameter. The characteristic frequency indicated is in dimensionless form following $\omega\varepsilon\varepsilon_0\rho_0$.

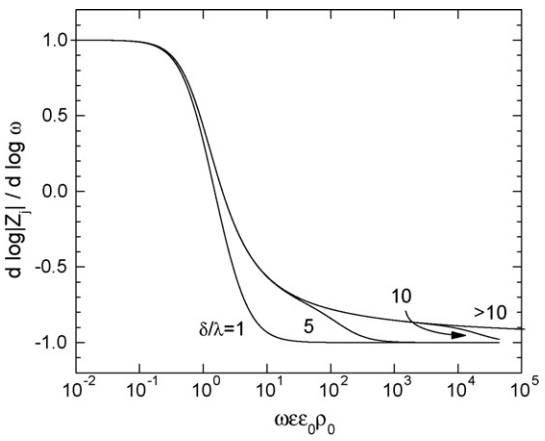

Fig. 9. The derivative of the logarithm of the magnitude of the imaginary part of the impedance with respect to the logarithm of frequency as a function of dimensionless frequency for the simulations presented in Fig. 8.

The result is

$$Z = -\frac{\lambda}{j\omega\varepsilon\varepsilon_0}\ln\left[\frac{1+j\omega\varepsilon\varepsilon_0\rho_0 e^{-\delta/\lambda}}{1+j\omega\varepsilon\varepsilon_0\rho_0}\right] \tag{33}$$

as was already calculated by Göhr et al. [63,64]. Eq. (33) is referred to as the Young impedance. In the low-frequency limit, application of L'Hôpitals rule yields

$$\lim_{\omega\to 0} Z = \lambda\rho_0(1-e^{-\delta/\lambda}) \tag{34}$$

This result is in agreement with the direct integration of resistivity which yielded Eq. (28). In the high-frequency limit,

$$\lim_{\omega\to\infty} Z = -j\frac{\delta}{\omega\varepsilon\varepsilon_0} \tag{35}$$

This result is also in agreement with direct integration of capacitance which yielded Eq. (31).

The impedance response associated with Eq. (33) is presented in Fig. 8 in dimensionless form with δ/λ as a parameter. The impedance was scaled by the zero-frequency asymptote given by Eq. (34). The characteristic frequency indicated in the figure is in dimensionless form following $\omega\varepsilon\varepsilon_0\rho_0$. For $\delta/\lambda = 1$, the peak in the imaginary impedance is slightly smaller than 0.5 and the Nyquist plot is only slightly depressed from perfect *RC* behavior. For larger values of δ/λ, distortion is evident at higher frequencies. The shape of the plot remains unchanged for $\delta/\lambda > 5$. The absence of time-constant dispersion at low frequencies indicates that the Young model cannot account for the low-frequency behavior for skin seen in Fig. 7(a).

To understand the relationship between Young impedance and CPE behavior, impedance values calculated according to Eq. (33) were analyzed by an R_f–CPE parallel combination, in series with the electrolyte resistance. The CPE parameters Q and α can be obtained following the graphical methods outlined by Orazem et al. [43]. The parameter α can be obtained from the slope of the imaginary part of the impedance plotted as a function of frequency in a logarithmic scale. The slope is presented in Fig. 9 as a function of dimensionless frequency $\omega\varepsilon\varepsilon_0\rho_0$. At low frequency, $d\log|Z_j|/d\log\omega = 1$, showing that the exponential decay of resistivity does not result in low-frequency time-constant dispersion. At high frequency and for $\delta/\lambda = 1$, $d\log|Z_j|/d\log\omega = -1$, again showing that the exponential decay of resistivity does not result in high-frequency time-constant dispersion. For larger values of δ/λ, a significant frequency range above $\omega\varepsilon\varepsilon_0\rho_0 = 1$ is seen for which $d\log|Z_j|/d\log\omega$ differs from -1.

The CPE parameters Q and α were determined graphically for each frequency above $\omega\varepsilon\varepsilon_0\rho_0 = 1$. The effective capacitance was calculated using Eq. (18), and the effective film thickness was calculated using Eq. (25). The results are presented in Fig. 10(a) as a function of dimensionless frequency and with δ/λ as a parameter. If the frequency is sufficiently large, the effective film thickness d_{eff} is equal to the actual film thickness δ for any value of δ/λ. For a broad frequency range and for $\delta/\lambda > 1$, the effective film thickness obtained from the capacitance can clearly be significantly smaller than the actual film thickness. For $\delta/\lambda = 400$, the effective film

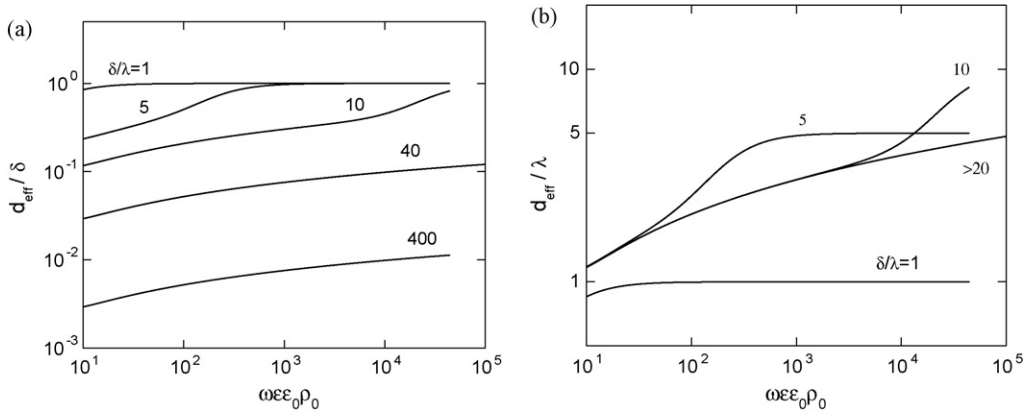

Fig. 10. The effective film thickness obtained for the simulations presented in Fig. 8 using Eqs. (18) and (25): (a) normalized by the known film thickness δ; and (b) normalized by the characteristic length λ.

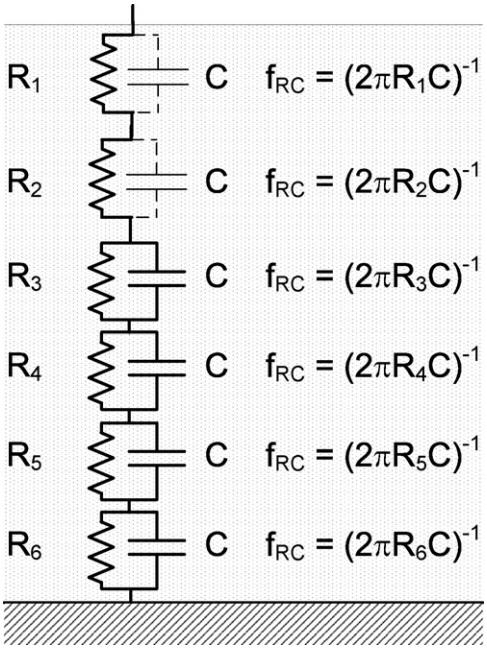

Fig. 11. Circuit representation of a normal distribution of resistivity in which some capacitance elements are not observed over an experimentally accessible frequency range due to local variation of resisitivity.

thickness is two orders of magnitude smaller than the actual film thickness for frequencies as high as $\omega\varepsilon\varepsilon_0\rho_0 = 10^5$.

The simulations show that, for $\delta/\lambda = 5$, the effective film thickness abruptly approaches the actual film thickness at $\omega\varepsilon\varepsilon_0\rho_0 = 10^2$. A similar abrupt change is seen for $\delta/\lambda = 10$ at $\omega\varepsilon\varepsilon_0\rho_0 = 10^4$. The simulations indicate that, while the capacitance obtained from the impedance response for a film with an exponential decay of resistivity should yield, in the limit of infinite frequency, the correct thickness of the film, measurement over a finite frequency range will yield a film thickness that is substantially smaller. As shown in Fig. 10(b), the effective film thickness is larger than the characteristic length λ. Thus, the film thickness obtained from the capacitance can lie between the actual film thickness δ and the characteristic length λ.

4. Discussion

The results presented above show that, while Eq. (25) will be valid in the limit of infinite frequency, a finite experimentally accessible frequency range may render undetectable the capacitance contributions from a portion of the film. This effect may be significant for cases where the local resistivity varies significantly with position. The effect is illustrated in Fig. 11. For a constant capacitance C and local resistance R_1, measurement at frequencies much below $\omega = 1/R_1C$ will yield only the resistance R_1 because the capacitor acts as an open circuit at these frequencies. In this case, represented by the upper two RC elements in Fig. 11, the effective capacitance obtained from Eq. (18) will under predict the thickness of the film. Only the most resistive part of the film is probed by impedance. The capacitance elements that are not observed by impedance can be either at the metal/film interface or at the film/electrolyte interface.

The consequence is explored here for the specific case of a film with a uniform dielectric constant and an exponential decay of resistivity. The dielectric response of both niobium oxide [47,59,60] and skin [61,62] have been described in terms of exponential decays of resistivity. Regression of such a model to the data obtained for anodic dissolution of niobium at a potential of 6 V(SCE) in an acid fluoride medium yielded, for $\varepsilon = 42$, values of $\rho_0 = 2.66 \times 10^9$ Ω cm, $\delta = 30$ nm, and $\lambda = 8$ nm. Under these conditions, the simulation of an exponential decay of resistivity indicates that, for frequencies above 5 kHz, $\alpha \approx 1$ and $d_{\text{eff}}/\delta \approx 1$. A comparison of the Young model to the impedance data for niobium oxide at a potential of 6 V(SCE), presented in Fig. 12(a), shows that the slope of the Young model is equal to unity for frequencies greater than 5 kHz. The disagreement between the value of $\alpha = 0.90$ obtained from experiment and the value of $\alpha = 1$ obtained from the model indicates that the exponential decay of resistivity provides only an approximate description of the high-frequency behavior of the Nb_2O_5. Nevertheless, the simulation value of $d_{\text{eff}}/\delta = 1$ is consistent with the good agreement found between the thickness estimated from the impedance measurement using Eqs. (18) and (25) and values obtained by independent methods.

In vivo impedance experiments obtained by tape-stripping successive layers of skin from human subjects demonstrated that the resistivity of human stratum corneum decays exponentially with position [61,62]. A Young model analysis was therefore performed for the in vitro data presented in Fig. 7 for heat-stripped human stratum corneum. Model parameters were obtained by matching the high-frequency portion of the impedance response given in Fig. 7. The model parameters ε, ρ_0, and λ were selected to match the zero-frequency asymptote for the real part of the impedance, match the characteristic frequency at which the imaginary part of the impedance had a maximum magnitude, and yield a dielectric constant between the dielectric constant of water ($\varepsilon = 80$) and lipid ($\varepsilon = 2$) [65]. The value of skin thickness was assumed to be either

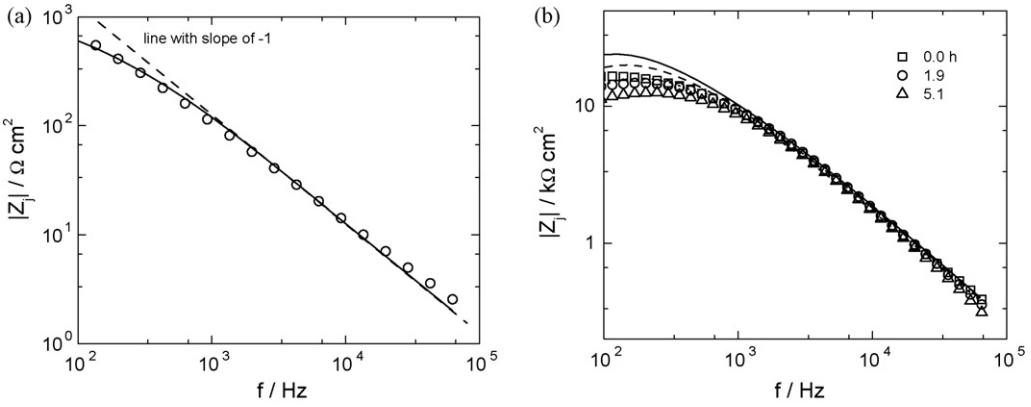

Fig. 12. Comparison of the Young model to the high-frequency part of the experimental imaginary part of the impedance as a function of frequency: (a) niobium oxide at a potential of 6 V(SCE) (see Fig. 6); and (b) human stratum corneum with immersion time as a parameter (see Fig. 7). The lines represent the model, and symbols represent the data.

Table 4
Physical properties obtained by matching the high-frequency portion of the impedance response given in Fig. 7 for heat-stripped human stratum corneum in 50 mM buffered $CaCl_2$ electrolyte as a function of immersion time.

Time/h	ρ_0/Ω cm	ε	δ/μm	λ/μm	α	d_{eff}/δ
0	6×10^8	49	20	1	0.848	0.152
0	6×10^8	49	40	1	0.858	0.078
1.9	5×10^8	49	20	1	0.844	0.143
1.9	5×10^8	49	40	1	0.854	0.076
5.1	4×10^8	49	20	1	0.839	0.139
5.1	4×10^8	49	40	1	0.850	0.074

20 μm or 40 μm, in keeping with reported values [61,62]. The comparison between the Young model and the data is given in Fig. 12(b), and the resulting parameters are presented in Table 4. The characteristic length $\lambda = 1$ μm is in agreement with the data presented by Kalia et al. [62], but is smaller than the value $\lambda = 5$ μm reported by Yamamoto and Yamamoto [61]. Values of $\lambda > 1.5$ yielded, for the present experimental data, dielectric constants that were greater than that of water.

The values of α and d_{eff}/δ reported in Table 4 were estimated from the simulation at a frequency of 50 kHz. This frequency was chosen for this analysis because it is at the upper limit of the experimental frequency range. As shown in Fig. 9, the Young model provides only a pseudo-CPE behavior over a broad high-frequency range in which the CPE parameters are weak functions of frequency. The good agreement between the value of α obtained from experiment and from the model suggests that the exponential decay of resistivity provides a good description for the high-frequency behavior of the skin. In addition, the simulation values for d_{eff}/δ are consistent with the observation that the thicknesses estimated from impedance measurements using Eqs. (18) and (25) were substantially smaller than those reported in the literature. The results presented here support the observation by Oh et al. that the capacitance of the skin could not be measured after repeated removal of skin layers reduced the impedance to a value indistinguishable from that of the bathing medium [66].

The resistivity profiles corresponding to the simulations presented in this section are given in Fig. 13. The change in resistivity for the Nb_2O_5 film is small enough that the entire dielectric response of the film can be seen in the experimental frequency range. In contrast, the change in local resistivity of the skin is much larger, and the capacitance associated with the region of smaller resistivity values is not seen in the experimental frequency range. Accordingly, the thickness estimated from the effective capacitance is much smaller than the actual thickness of the skin. In this case, the thickness obtained from impedance measurements is the thickness of the higher resistivity region. As illustrated in Fig. 10 for the Young model, δ/λ is the key parameter for determining the meaning of the effective film thickness. When δ/λ is small, the effective thickness determined from the capacitance is the actual film thickness. When δ/λ is large, the effective thickness determined from the capacitance is the thickness of only the resistive portion of the film.

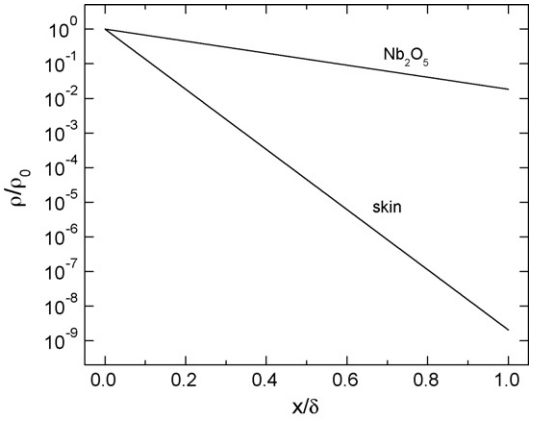

Fig. 13. Resistivity profiles associated with the simulation of the impedance response for Nb_2O_5 at 6 V(SCE) and skin using a uniform dielectric constant and an exponentially decaying resistivity.

5. Conclusions

Methods for determination of effective capacitance from CPE parameters have been employed extensively in the impedance literature. It is not obvious that all the authors who used the relationships derived by Brug et al. [1] and presented by Hsu and Mansfeld [11] were fully aware that the former are appropriate only for a surface distribution of time constants and the latter applies only to a normal distribution, as is demonstrated in the present work. The present results illustrate the importance of using the correct formula that corresponds to a given type of distribution. Misuse of the formulas, for example by using an incorrect effective resistance in the C_{eff} calculation, may lead to macroscopic errors, since the values of electrolyte resistance, charge-transfer resistance and film resistance may be quite different. The selection of the right formula should rest on the knowledge of the system under investigation, obtained by different methods. For instance, local impedance may provide evidence for surface/normal inhomogeneity; whereas, spectroscopic methods may show the presence of films for which properties might be distributed in the normal direction.

The effective capacitance obtained for a normal distribution can yield correct values for the film thickness under conditions where the local resistivity does not vary significantly. When the local resistivity varies considerably over the thickness of a film, the experimental frequency range may preclude observation of the capacitance contribution of a portion of the film. In this case, the effective capacitance obtained from impedance measurements will under-predict the film thickness. The value of film thickness obtained from impedance data for such systems should be interpreted as being the thickness of the high-resistivity region that is accessible to the impedance measurement.

Acknowledgements

Mark Orazem acknowledges helpful exchanges with Professor Annette Bunge and Erick White (Colorado School of Mines, Golden Colorado) that motivated the simulations used to interpret the impedance of skin.

References

[1] G.J. Brug, A.L.G. van den Eeden, M. Sluyters-Rehbach, J.H. Sluyters, J. Electroanal. Chem. 176 (1984) 275.
[2] J.R. Macdonald, Impedance Spectroscopy: Emphasizing Solid Materials and Systems, John Wiley & Sons, New York, 1987.
[3] A. Lasia, in: R.E. White, B.E. Conway, J.O.M. Bockris (Eds.), Modern Aspects of Electro-chemistry, vol. 32, Plenum Press, New York, 1999, p. 143.
[4] Z. Lukacs, J. Electroanal. Chem. 432 (1997) 79.
[5] Z. Lukacs, J. Electroanal. Chem. 464 (1999) 68.
[6] J.R. Macdonald, J. Appl. Phys. 58 (5) (1985) 1971.
[7] J.R. Macdonald, J. Appl. Phys. 58 (5) (1985) 1955.
[8] R.L. Hurt, J.R. Macdonald, Solid State Ionics 20 (1986) 111.
[9] J.R. Macdonald, J. Appl. Phys. 62 (11) (1987) R51.
[10] J.R. Macdonald, J. Electroanal. Chem. 378 (1994) 17.
[11] C.H. Hsu, F. Mansfeld, Corrosion 57 (2001) 747.
[12] V.M.-W. Huang, V. Vivier, M.E. Orazem, N. Pébère, B. Tribollet, J. Electrochem. Soc. 154 (2007) C81.
[13] V.M.-W. Huang, V. Vivier, M.E. Orazem, N. Pébère, B. Tribollet, J. Electrochem. Soc. 154 (2007) C99.
[14] W.G. Pell, A. Zolfaghari, B.E. Conway, J. Electroanal. Chem. 532 (1–2) (2002) 13.

[15] V.D. Jović, B.M. Jović, J. Electroanal. Chem. 541 (2003) 1.
[16] V.D. Jović, B.M. Jović, J. Electroanal. Chem. 541 (2003) 13.
[17] P.S. Germain, W.G. Pell, B.E. Conway, Electrochim. Acta 49 (11) (2004) 1775.
[18] M. Figueiredo, C. Gomes, R. Costa, A. Martins, C.M. Pereira, F. Silva, Electrochim. Acta 54 (9) (2009) 2630.
[19] C. Gabrielli, P.P. Grand, A. Lasia, H. Perrot, J. Electrochem. Soc. 151 (11) (2004) A1943.
[20] M.H. Martin, A. Lasia, Electrochim. Acta 54 (22) (2009) 5292.
[21] L.L. Chen, A. Lasia, J. Electrochem. Soc. 138 (1991) 3321.
[22] H. Dumont, P. Los, L. Brossard, A. Lasia, H. Ménard, J. Electrochem. Soc. 139 (8) (1992) 2143.
[23] H.J. Miao, D.L. Piron, Electrochim. Acta 38 (8) (1993) 1079.
[24] N.R. Elezović, V.D. Jović, N.V. Krstajić, Electrochim. Acta 50 (28) (2005) 5594.
[25] L. Vázquez-Gómez, S. Cattarin, P. Guerriero, M. Musiani, Electrochim. Acta 52 (2007) 8055.
[26] S.M.A. Shibli, V.S. Dilimon, Int. J. Hydrogen Energy 33 (4) (2008) 1104.
[27] V.A. Alves, L.A. da Silva, J.F.C. Boodts, Electrochim. Acta 44 (8–9) (1998) 1525.
[28] R. Jurczakowski, C. Hitz, A. Lasia, J. Electroanal. Chem. 572 (2004) 355.
[29] J.M. Campiña, A. Martins, F. Silva, J. Phys. Chem. C 111 (14) (2007) 5351.
[30] J.M. Campiña, A. Martins, F. Silva, J. Phys. Chem. C 113 (6) (2009) 2405.
[31] T. Zalewska, A. Lisowska-Oleksiak, S. Biallozor, V. Jasulaitiene, Electrochim. Acta 45 (24) (2000) 4031.
[32] S.P. Harrington, T.M. Devine, J. Electrochem. Soc. 155 (2008) C381.
[33] S.P. Harrington, T.M. Devine, J. Electrochem. Soc. 156 (4) (2009) C154.
[34] V.D. Jović, B.M. Jović, Corros. Sci. 50 (2008) 3063.
[35] T. Van Schaftinghen, C. Le Pen, H. Terryn, F. Hrzenberger, Electrochim. Acta 49 (17–18) (2004) 2997.
[36] M.L. Zheludkevich, R. Serra, M.F. Montemor, K.A. Yasakau, I.M.M. Salvado, M.G.S. Ferreira, Electrochim. Acta 51 (2) (2005) 208.
[37] T. Van Schaftinghen, C. Deslouis, A. Hubin, H. Terryn, Electrochim. Acta 51 (8–9) (2006) 1695.
[38] K.A. Yasakau, M.L. Zheludkevich, O.V. Karavai, M.G.S. Ferreira, Prog. Org. Coat. 63 (2008) 352.
[39] M.L. Zheludkevich, K.A. Yasakau, S.K. Poznyak, M.G.S. Ferreira, Corros. Sci. 47 (2005) 3368.
[40] E. Chassaing, B. Sapoval, G. Daccord, R. Lenormand, J. Electroanal. Chem. 279 (1–2) (1990) 67.
[41] E.D. Bidóia, L.O.S. Bulhões, R.C. Rocha-Filho, Electrochim. Acta 39 (5) (1994) 763.
[42] V.M.-W. Huang, V. Vivier, I. Frateur, M.E. Orazem, B. Tribollet, J. Electrochem. Soc. 154 (2007) C89.
[43] M.E. Orazem, N. Pébère, B. Tribollet, J. Electrochem. Soc. 153 (2006) B129.
[44] S. Cattarin, M. Musiani, B. Tribollet, J. Electrochem. Soc. 149 (10) (2002) B457.
[45] M. Bojinov, Electrochim. Acta 42 (23–24) (1997) 3489.
[46] M. Bojinov, J. Solid State Electrochem. 1 (1997) 161.
[47] I. Frateur, ECS Trans. 13 (13) (2008) 115.
[48] J.J. Randall, W.J. Bernard, R.R. Wilkinson, Electrochim. Acta 10 (2) (1965) 183.
[49] F. Di Quarto, S. Piazza, C. Sunseri, Electrochim. Acta 35 (1) (1990) 99.
[50] M.M. Lohrengel, Mater. Sci. Eng. R11 (1993) 243.
[51] I. Arsova, L. Arsov, N. Hebestreit, A. Anders, W. Plieth, J. Solid State Electrochem. 11 (2007) 209.
[52] H. Habazaki, T. Ogasawara, H. Konno, K. Shimizu, K. Asamic, K. Saito, S. Nagata, P. Skeldon, G.E. Thompson, Electrochim. Acta 50 (2005) 5334.
[53] A. Heidelberg, C. Rozenkranz, J.W. Schultze, T. Schäpers, G. Staikov, Surface Science 597 (2005) 173.
[54] M.A. Membrino, Transdermal delivery of therapeutic drugs by iontophoresis, Ph.D. Thesis, University of Florida, Gainesville, FL, December 2001.
[55] L.L. Langley, I. Telford, J.B. Christensen, Dynamic Anatomy and Physiology, 4th edition, McGraw-Hill, New York, 1974.
[56] P.T. Wojcik, P. Agarwal, M.E. Orazem, Electrochim. Acta 41 (7/8) (1996) 977.
[57] P.T. Wojcik, M.E. Orazem, Corrosion 54 (1998) 289.
[58] G.F. Odland, in: L.A. Goldsmith (Ed.), Biochemistry and Physiology of the Skin, Oxford University Press, New York, 1991, p. 3 (Chapter 1).
[59] L. Young, Trans. Faraday Soc. 51 (1955) 1250.
[60] L. Young, Anodic Oxide Films, Academic Press, New York, 1961.
[61] T. Yamamoto, Y. Yamamoto, Med. Biol. Eng. 14 (1976) 151.
[62] Y.N. Kalia, F. Pirot, R.H. Guy, Biophys. J. 71 (1996) 2692.
[63] H. Göhr, Ber. Bunsenges. Phys. Chem. 85 (1981) 274.
[64] H. Göhr, J. Schaller, C.A. Schiller, Electrochim. Acta 38 (14) (1993) 1961.
[65] U. Pliquett, R. Langer, J.C. Weaver, Biochim. Biophys. Acta 1239 (2) (1995) 111.
[66] S.Y. Oh, L. Lyung, D. Bommannan, R.H. Guy, R.O. Potts, J. Control. Release 27 (27) (1993) 115.